Coherent optical creation of a single molecule

Yichao Yu,[1,2,3,*] Kenneth Wang,[1,2,3,*] Jonathan D. Hood,[4] Lewis R. B. Picard,[1,2,3] Jessie T. Zhang,[1,2,3] William B. Cairncross,[2,1,3] Jeremy M. Hutson,[5] Rosario Gonzalez-Ferez,[6,7] Till Rosenband,[8] and Kang-Kuen Ni[2,1,3,†]

[1]*Department of Physics, Harvard University, Cambridge, Massachusetts 02138, USA*
[2]*Department of Chemistry and Chemical Biology, Harvard University, Cambridge, Massachusetts 02138, USA*
[3]*Harvard-MIT Center for Ultracold Atoms, Cambridge, Massachusetts 02138, USA*
[4]*Department of Chemistry, Purdue University, West Lafayette, Indianna, 47906, USA*
[5]*Joint Quantum Centre Durham-Newcastle, Department of Chemistry, Durham University, Durham, DH1 3LE, United Kingdom*
[6]*Instituto Carlos I de Física Teórica y Computacional, and Departamento de Física Atómica, Molecular y Nuclear, Universidad de Granada, 18071 Granada, Spain*
[7]*ITAMP, Harvard-Smithsonian Center for Astrophysics, Cambridge, Massachusetts 02138, USA*
[8]*Agendile LLC, Cambridge, Massachusetts 02139, USA*

(Dated: December 15, 2020)

We report coherent association of atoms into a single weakly bound NaCs molecule in an optical tweezer through an optical Raman transition. The Raman technique uses a deeply bound electronic excited intermediate state to achieve a large transition dipole moment while reducing photon scattering. Starting from two atoms in their relative motional ground state, we achieve an optical transfer efficiency of 69%. The molecules have a binding energy of 770.2 MHz at 8.83(2) G. This technique does not rely on Feshbach resonances or narrow excited-state lines and may allow a wide range of molecular species to be assembled atom-by-atom.

Diverse species of fully quantum-controlled ultracold molecules are desired for a variety of applications including precision measurements [1–6], quantum simulations [7–10], quantum information processing [11–14], and studies of ultracold chemistry [15–18]. While many innovative approaches in the last few years have directly cooled different species of molecules below 1 mK [19–24], the highest phase-space-density gas [25] and trapped individual molecules [26, 27] have been achieved through the association of ultracold atoms.

Molecular association of ultracold atoms takes advantage of the cooling and trapping techniques that have been developed for atoms. Associating atoms into deeply bound molecules is challenging because of the small wavefunction overlap between the free-atom and molecular states and the release of large binding energy. A widely used method of overcoming these challenges is to associate atom pairs into weakly bound molecules first, and then transfer the molecules from this single internal state to a desired rovibrational and electronic state, releasing the binding energy by stimulated emission [1, 28–35]. So far, molecular association has generally been achieved by magnetoassociation through a magnetic Feshbach scattering resonance. Exceptions include Sr_2, where narrow-linewidth ($\sim$ 20 kHz) excited states are available and optical association can be driven coherently [36, 37], and ^{87}Rb^{85}Rb with molecular states bound by only $1-2$ MHz [27]. With these requirements, molecules involving non-magnetic atoms [38] or atoms without narrow intercombination lines remain difficult to associate.

Here, we demonstrate coherent association of an atom pair to a weakly bound molecule by two-photon optical Raman transfer via an electronic excited state, as shown in Fig. 1a, taking NaCs as the prototype system. The technique does not rely on a Feshbach resonance, molecular states bound by a only few MHz, or a narrow excited state. The resulting single molecule is in a well-defined internal quantum state and predominantly in its motional ground state. A vibrational state of the electronic excited state $c^3\Sigma^+(\Omega = 1)$ serves as the intermediate state in the Raman technique, and is chosen to minimize photon scattering during Raman Rabi oscillations. To reduce photon scattering and sensitivity to laser intensity noise further, we choose the initial and final states that balance the two Rabi frequencies as much as possible. This approach applies to a variety of molecules that can be created atom-by-atom with full quantum-state control.

The optical Raman transfer is illustrated by the idealized three-level system shown in Fig. 1a, where the initial atomic state and the target weakly bound molecular state are coupled to an intermediate state by two lasers with Rabi frequencies Ω_a and Ω_m, one-photon detuning Δ, and all Rabi frequencies are population oscillation frequencies. The transfer Raman Rabi frequency is given by $\Omega_a\Omega_m/(2\Delta)$ [39]. Unlike Raman transitions in atoms, the one-photon Rabi frequencies are greatly imbalanced ($\Omega_a/\Omega_m \ll 1$) due to the small wavefunction overlap between the atomic state and the intermediate state, and scattering losses are dominated by the final state. Because the energy difference between the atomic state and target molecular state is small (< 1 GHz) compared to the single-photon detuning of 80 to 200 GHz, both beams

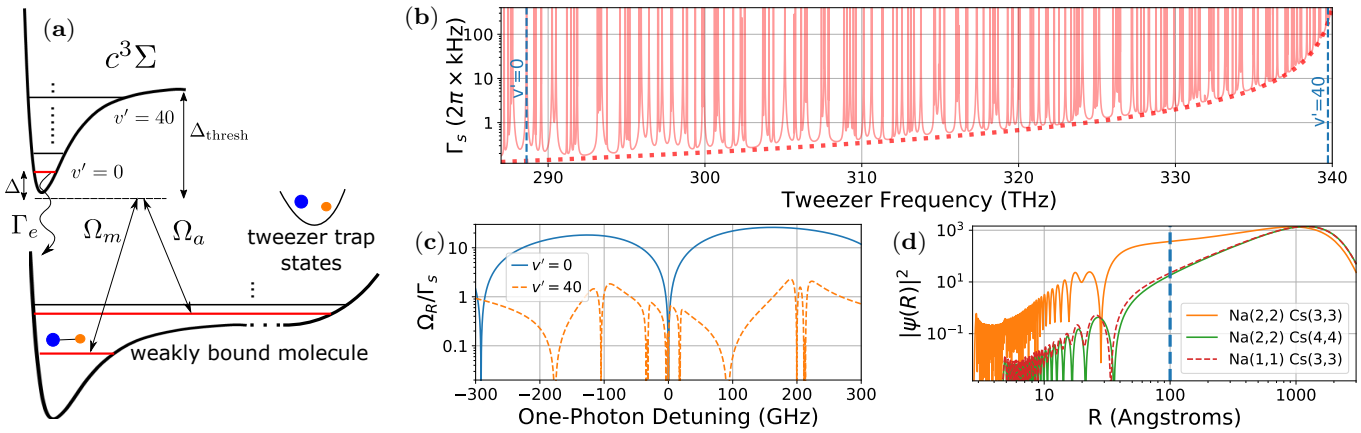

FIG. 1. Optical creation of single molecules from single atoms in an optical tweezer. (a) Schematic of the optical transition from an atom pair to a weakly bound molecule. The initial state is the relative motional ground state between the two atoms and the final state is the first molecular bound state. The transition is driven by a pair of laser frequencies whose difference (< 1 GHz) matches the molecular binding energy. The lasers are detuned by Δ from an excited vibrational sublevel in the $c^3\Sigma^+(\Omega = 1)$ electronic state in order to reduce scattering during the transfer. (b) Calculation of the scattering rate vs. laser frequency including all vibrational states of 8 excited-state potentials and the atomic continuum. The assumed excited-state linewidth for molecular lines is 50 MHz. The dotted red line shows the contribution from the near-threshold states, which approximately scales as $1/\Delta^2_{\rm thresh}$. (c) Comparison between vibrational sublevels of the intermediate excited state for the Raman transition. The lowest sublevel (blue) has a larger optimum ratio of Raman Rabi frequency to scattering rate than the higher sublevel (orange). (d) The large scattering length for $\mathrm{Na}(2,2), \mathrm{Cs}(3,3)$ is associated with enhancement of the relative wavefunction at short internuclear distance (R).

scatter nearly equally with a total rate $\Gamma_{\rm e}\Omega_{\rm m}^2/(2\Delta^2)$, where $\Gamma_{\rm e}$ is the excited-state linewidth. The two beams have equal power to maximize the Raman Rabi frequency at fixed total power. In this idealized treatment, the ratio between the Raman Rabi frequency and the scattering rate is $\Omega_{\rm a}/\Omega_{\rm m} \times \Delta/\Gamma_{\rm e}$, which limits the transfer efficiency into the molecular state. At the same time, the intensity-stability requirement is determined by the ratio of Raman Rabi frequency to light shift $\Omega_{\rm a}/\Omega_{\rm m}$. Notably, both figures of merit improve with a larger ratio $\Omega_{\rm a}/\Omega_{\rm m}$.

Earlier experiments used excited states with high vibrational quantum number for the intermediate state of the Raman transition to ensure a large Raman Rabi frequency [40, 41]. However, a complete picture includes both the many vibrational levels of the excited electronic state and the atomic continuum. Then the scattering and Raman Rabi rates are sums over all possible intermediate states. As there is large overlap between the target molecular state and other vibrationally excited states, intermediate states that are closer to the dissociation threshold result in a large scattering rate. This scattering is approximately proportional to $1/\Delta^2_{\rm thresh}$, where $\Delta_{\rm thresh}$ is the detuning from the dissociation threshold, which is smaller for intermediate states that are deeply bound.

We optimize over intermediate states by calculating the total Raman Rabi frequency $\Omega_{\rm R}$ and scattering rate $\Gamma_{\rm s}$ at different detunings from the atomic threshold, taking into account all states of 8 excited molecular electronic potentials [42–46] and the continuum [47]; see Supplementary Material for details. This calculation shows that the figure of merit $\Omega_{\rm R}/\Gamma_{\rm s}$ can be larger for the lowest vibrational state compared to higher bound states at a cost of a smaller transfer rate $\Omega_{\rm R}$, as shown in Fig. 1c. As a result, we choose the $v' = 0$ level of $c^3\Sigma^+(\Omega = 1)$ as the intermediate state near which to drive Raman transitions.

In addition to the intermediate state, the choice of initial and final Zeeman and hyperfine states affects the single-photon rates $\Omega_{\rm a}$ and $\Omega_{\rm m}$. Due to the small extent of the intermediate-state wavefunction compared to that of the trapped atoms, $\Omega_{\rm a}$ is approximately proportional to the amplitude of the relative atomic wavefunction at short distance, within the range of the molecular potential. To increase this amplitude, one can increase the external confinement of atom pairs. In a harmonic approximation the short-range amplitude is proportional to $\omega_{\rm trap}^{3/4}$ or $P^{3/8}$, where $\omega_{\rm trap}$ is the trap frequency and P is the optical power in the tweezer trap [48] with a fixed beam waist. However, additional power may not be available and also leads to additional undesired scattering. Alternatively, one can choose an atomic pair state with a large scattering length (positive or negative). For such states, the amplitude of the relative atomic wavefunction is substantially enhanced at short range, as shown in Fig. 1d. For our system of Na and Cs atoms, we choose a spin-state combination $|{\uparrow_{\rm Na}}{\downarrow_{\rm Cs}}\rangle \equiv |f = 2, m_f = 2\rangle_{\rm Na} |f = 3, m_f = 3\rangle_{\rm Cs}$ that has a large and negative scattering length of $a({\uparrow_{\rm Na}}{\downarrow_{\rm Cs}}) \approx -700 a_0$ [49]. All other stable spin combinations give smaller scatter-

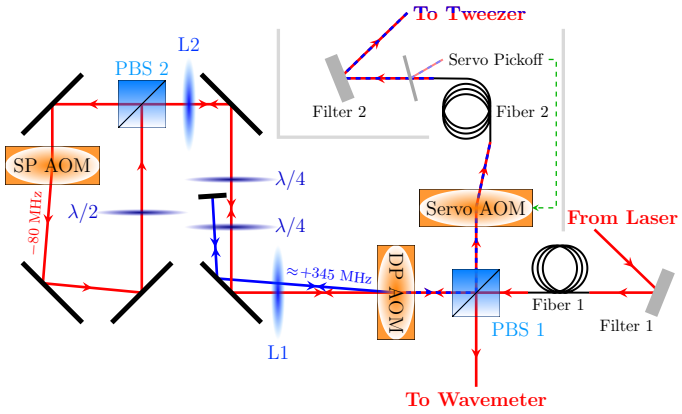

FIG. 2. Beam path for generating two frequencies in the tweezer for the Raman transition (only essential optics shown.) Two filters, one directly after the laser source and one after both optical fibers clean the light from a fiber amplifier seeded by an external cavity diode laser. The red beam path is the always-present 0^{th} order of the double pass (DP) AOM. The blue beam path is the switchable 1^{st} order of the DP AOM. It generates the second frequency for the Raman transition. To reduce interferences that cause relative power fluctuation of the two frequencies, the 0^{th} order is frequency shifted by −80 MHz before recombination. The experiment typically starts with the single-pass (SP) AOM on and the DP AOM off. When driving the Raman transition, the RF powers for both AOMs are ramped simultaneously to achieve the desired optical power at both frequencies, while keeping the total optical power fixed.

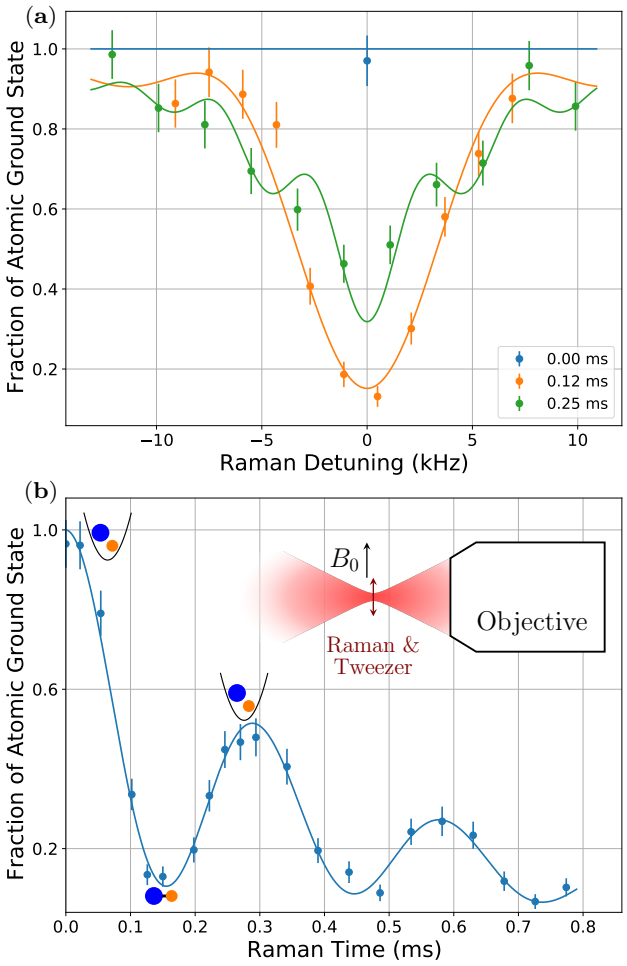

FIG. 3. Coherent transfer of atoms to molecules. The molecular state is dark to the imaging step and corresponds to zero signal. (a) Raman difference frequency scans for various durations showing the resonance as a function of the detuning from the fitted resonance at 770.5715(1) MHz, near the calculated value of 763 MHz. (b) Raman pulse-length scan on resonance. A decaying Rabi oscillation shows the coherence of the Raman transfer process. A model is fitted to (a) and (b) to determine the Raman Rabi frequency and loss rates. *Inset:* Geometry and polarization of trap and Raman beam relative to the magnetic field. The 3.25 mW beam is focused to a waist of 0.9 μm that confines the atoms and molecule. A perpendicular $B_0 = 8.83(2)$ G magnetic field defines the quantization axis and the atoms experience predominantly π-polarized light.

ing lengths ($< 50\ a_0$).

To identify a suitable target molecular state, we carry out coupled-channel calculations of the near-threshold bound states, as described in the Supplemental Material. Choosing a bound state with similar spin character to the atomic state minimizes the sensitivity of the transition frequency to magnetic field. A suitable state with this character is predicted about 763 MHz below the $|{\uparrow_{\text{Na}}}{\downarrow_{\text{Cs}}}\rangle$ threshold and the ratio $\Omega_{\text{a}}/\Omega_{\text{m}}$ increases to about 0.013. Compared to $\Omega_{\text{a}}/\Omega_{\text{m}} \approx 0.003$ for other combinations, this relaxes the intensity stability requirement to the percent level and enhances the Raman Rabi frequency.

Experimentally, we first prepare two atoms in a well-defined external and internal quantum state by using techniques developed previously [50–52]. In brief, the experimental cycle begins by stochastically loading a single ^{23}Na atom and a single ^{133}Cs atom into separate optical tweezers. The atoms are initially imaged to post-select loading of both atoms vs. none or one atom. After imaging, we turn on a 8.83(2) G magnetic field to define the quantization axis for the state preparation and molecule formation steps. Raman sideband cooling then prepares both atoms simultaneously in the 3-dimensional motional ground state of their optical tweezers, leaving the atoms in the spin state $|{\uparrow_{\text{Na}}}{\uparrow_{\text{Cs}}}\rangle \equiv |f=2, m_f=2\rangle_{\text{Na}} |f=4, m_f=4\rangle_{\text{Cs}}$, which has a small scattering length. The weak two-atom interaction allows merging of the two tweezers with minimum pertubation so that they remain in the motional ground state.

After merging the tweezers, we drive the atoms into spin combination $|{\uparrow_{\text{Na}}}{\downarrow_{\text{Cs}}}\rangle$ with a large scattering length by performing a Cs spin flip while taking into account the −30.7 kHz interaction shift [49]. This is the initial atomic state for Raman transfer. The spin flip selectively

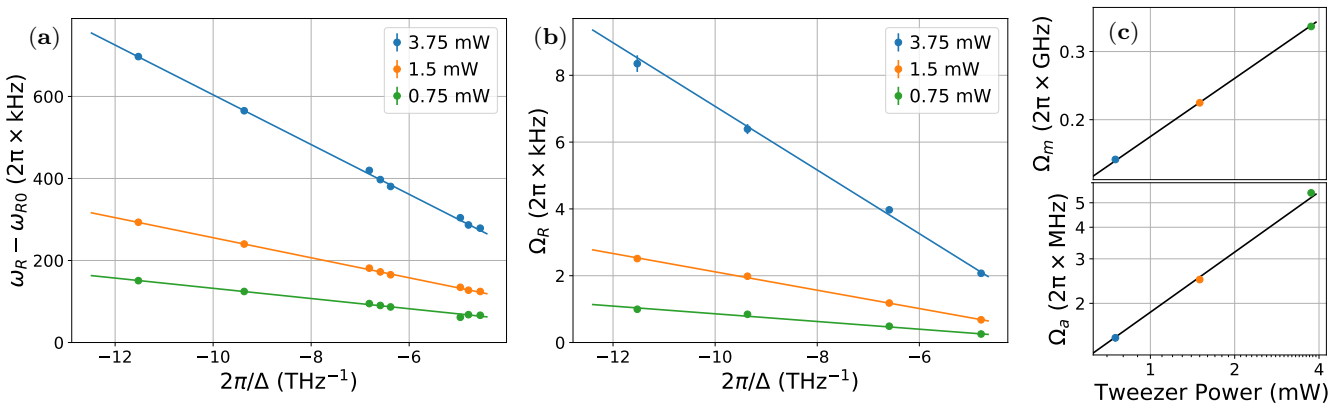

FIG. 4. Raman transition parameters as a function of tweezer power and detuning. (a) The Raman resonance ω_{R} fitted to $a_P + b_P/\Delta$, where a_P and $b_P = (\Omega_{\mathrm{a}}^2 - \Omega_{\mathrm{m}}^2)/2$ are the power (P) dependent background and $v' = 0$ contributions to the light shift and $\Delta \equiv 2\pi \times (f_{\mathrm{PA0}} - f_{\mathrm{tweezer}})$ is the detuning from the $v' = 0$ resonance frequency f_{PA0}. a_P is fitted to a model including linear and small quadratic light shift to obtain the Raman resonance frequency at zero tweezer power $\omega_{\mathrm{R0}} = 2\pi \times 770.1969(2)$ MHz where the statistical uncertainty is shown. (b) Raman Rabi frequency Ω_{R} fitted to $c_P + d_P/\Delta$, where c_P and $d_P = \Omega_{\mathrm{a}}\Omega_{\mathrm{m}}/2$ are the background and $v' = 0$ contributions that scale as $P^{1.29}$. The detuning is calculated from f_{PA0} fitted in (a). Fit parameters are listed in Table I. (c) Tweezer power dependency of Ω_{m} (top) and Ω_{a} (bottom) calculated from b_P and d_P on a log-log scale showing approximate $P^{0.5}$ scaling of Ω_{m} and $P^{0.79}$ scaling of Ω_{a}.

transfers atoms in the relative motional ground state, removing any background from atoms in excited states of relative motion [53]. For the experiment reported here, 31% of initial two-atom population is transferred. Of this population, over 60% is in the ground state of center-of-mass motion, inferred from Raman sideband thermometry.

To transfer the atom pair into the target weakly bound molecular state, we modulate the tweezer beam with a second frequency near 770 MHz, as shown in Fig. 2. The dual use of the tweezer beam for confinement and Raman transfer not only minimizes photon scattering, but also allows a tight focus to minimize the transfer duration. A tweezer frequency far detuned (by −151 GHz) from $v' = 0$ (< 50 MHz natural linewidth) reduces resonant scattering [51]. Furthermore, two filters, each with a linewidth (FWHM) of 50 GHz, clean the laser spectrum and prevent broadband noise from causing unwanted excitation. As shown in Fig. 2, one filter immediately follows the laser, while the second filter precedes the focusing objective for final cleanup of the laser spectrum.

Figure 3 shows a Fourier-limited resonance together with Rabi oscillations between the atomic and molecular states. A decaying Rabi oscillation with frequency $2\pi \times 3.28(4)$ kHz fitted to the data suggests that 69 % of atoms are transferred into the molecular state after a π-pulse, with the majority of molecules in the ground state of motion [26, 27].

To understand the details and limitations of the Raman transfer process better, we measured the properties of the two-photon resonance as a function of tweezer power and single-photon detuning. Known dependencies of the light shift and Raman Rabi frequency Ω_{R} on detuning Δ allow experimental determination of the Rabi frequencies Ω_{a} and Ω_{m} whose ratio critically affects the transfer efficiency. Both the light shift and Ω_{R} follow a $1/\Delta$ slope as shown in Fig. 4a, b and include a constant offset that we attribute to coupling to other excited states that are further away in energy. The $1/\Delta$ components due to the nearby $v' = 0$ intermediate state determine Ω_{m} and Ω_{a} in Table I.

P (mW)	0.75	1.5	3.75
f_{PA0} (GHz)	288711.8		
a ($2\pi \times$ MHz)	770.20452(6)	770.2081(1)	770.1943(3)
b ($4\pi^2 \times$ MHz · GHz)	−12.46(2)	−24.44(3)	−60.66(8)
c ($2\pi \times$ kHz)	0.29(2)	0.63(4)	2.4(2)
d ($4\pi^2 \times$ MHz · GHz)	0.115(4)	0.275(6)	0.95(3)
Ω_{R} ($2\pi \times$ kHz)	0.49(2)	1.18(3)	3.97(9)
Ω_{m} ($2\pi \times$ MHz)			348.3(3)
Ω_{a} ($2\pi \times$ kHz)			5.5(2)

TABLE I. Fitting results for Fig. 4(a,b). Ω_{R} is reported at −151 GHz detuning from the $v' = 0$ state. At 3.75 mW, $\Omega_{\mathrm{m}}/\Omega_{\mathrm{a}} = 0.016$, near the theory prediction of 0.013. The measured Rabi rate Ω_{R} is only 63 % of $\Omega_{\mathrm{m}}\Omega_{\mathrm{a}}/(2\Delta)$ due to interference from further-detuned Raman processes.

Figure 4c shows the power dependence of Ω_{m} and Ω_{a}, where Ω_{m} scales as $P^{1/2}$ as expected. As discussed previously, the scaling of Ω_{a} is $P^{7/8}$ for weakly interacting particles. However, due to the strong interaction between the two atoms in the $|{\uparrow_{\mathrm{Na}}}{\downarrow_{\mathrm{Cs}}}\rangle$ state, this approximation breaks down. Coupled-channel calculations show that the wavefunction scaling is well approximated by $P^{0.29}$

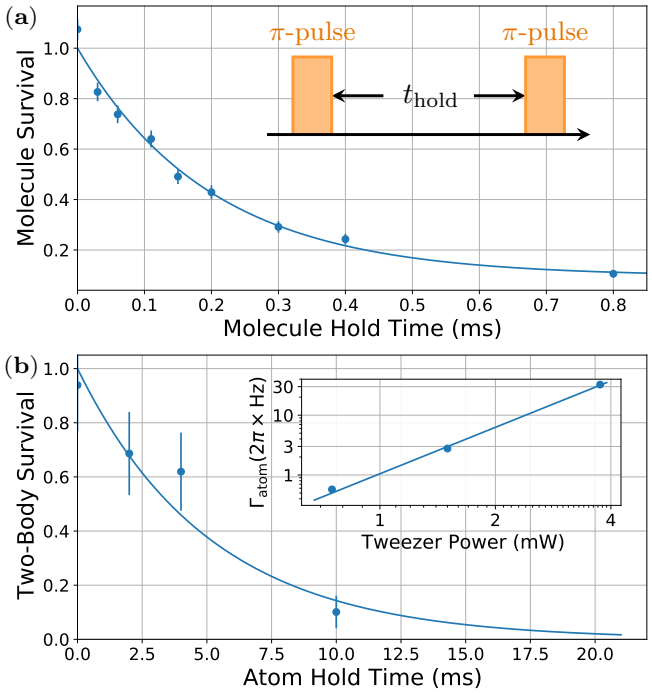

FIG. 5. Lifetime measurements with about 3.25 mW optical power. (a) Direct measurement of molecule lifetime. Molecule survival is detected by dissociating back to atoms via a second Raman transition. The lifetime is consistent with the decay of the Rabi oscillation in Fig. 3b. Inset: pulse sequence for the lifetime measurement. (b) Two-body atom lifetime of 5(1) ms limited by off-resonance photoassociation. This is used to improve the fitting of the Raman transfer data. Inset: Atomic scattering rate scales as $P_{\rm tweezer}^{2.58} \times 2\pi \times 1.05(6)$ Hz/mW$^{2.58}$ on a log-log scale; this is consistent with a two-photon scattering process.

within the range of confinement in our experiment and the expected scaling of $\Omega_{\rm a} \propto P^{0.79}$ agrees with the data.

While the measured single-photon Rabi frequencies of Table I are in broad agreement with calculations (see Supplementary Materials), calculated scattering rates of the molecular and atomic state underestimate the decoherence in Fig. 3b. From experimental measurements, the Raman transfer efficiency is limited by the molecular lifetime, together with a reduction in the Raman Rabi frequency due to destructive interference with intermediate states beyond $v' = 0$ (see Table I). We discuss loss and decoherence below.

The molecular lifetime measurement in Fig. 5a is performed by preparing the molecule with a π-pulse, followed after a variable delay by a second dissociating π-pulse. The measured lifetime of 0.196(14) ms is consistent with the decaying time scale of 0.203(13) ms of the Rabi oscillation in Fig. 3b. Preliminary experiments and theoretical considerations indicate that the molecular lifetime may be limited by two-photon coupling to the atomic continuum [54]. Atom loss is shown to be small in Fig. 5b by measuring the two-body lifetimes of the atoms directly without the second Raman frequency. In principle, destructive interference that reduces the Raman Rabi rate $\Omega_{\rm R}$ for negative detunings Δ changes to constructive interference for positive detunings, but additional molecular resonances make the positive region unusable. More negative detunings that might reduce the scattering rate were prevented by vanishing of $\Omega_{\rm R}$.

Separately we observe a decrease in coherence by a factor of 2 without laser spectrum filters, suggesting that spectral impurity of the laser can be a significant source of loss. While we have not fully characterized the sources of broadband noise, possibilities include amplified spontaneous emission (ASE) from the laser and fiber nonlinearities. Other potential decoherence sources include fluctuations of the tweezer intensity and magnetic field, although the shape of the Rabi oscillation in Fig. 3b indicates that loss rather than frequency fluctuations are responsible for decoherence. Based on the ratio between $\Omega_{\rm R}$ and the light shift, the requirement on the tweezer intensity stability is 1% at 3.75 mW power. We stabilize the power to 0.1%, indicating that in the absence of beam-waist fluctuations, light shift is not a major source of decoherence. Similarly, the measured Zeeman shift of 42.2(2) kHz/G does not cause significant decoherence for the measured magnetic field fluctuation of 1.5 mG.

In conclusion, we have coherently formed a weakly bound NaCs molecule in an optical tweezer by optical Raman transfer. This process is enabled by utilizing a deeply-bound intermediate state, as well as highly-interacting initial atomic states. A theoretical investigation including 8 excited molecular electronic potentials, the electronically excited atomic continuum, and coupled-channel ground-state wavefunctions indicates the potential for higher transfer efficiency than the observed value of 69 %. Future experiments may benefit from better balancing of the up-leg and down-leg Rabi frequencies, for example by driving to more deeply bound states. If possible, destructive interference that reduces the two-photon Rabi rate should be avoided. Nonlinear optical effects that limit the molecular state lifetime can also be explored.

Our technique can be applied to form a diverse set of molecular species, because it does not rely on a magnetic Feshbach resonance, states bound by only a few MHz, or a narrow excited state. The formation of weakly bound molecules is a key step in forming rovibrational ground-state molecules. By scaling up to many optical tweezers [55–57], large arrays with arbitrary geometry of highly controlled molecules can be achieved. These molecules comprise a flexible platform for quantum simulation, quantum computing, precision measurements applications.

We thank Bo Gao and Paul Julienne for discussion and Robert Moszynski for providing theoretical transition dipole moments of NaCs. This work is supported by the NSF (PHY-1806595), the AFOSR (FA9550-19-1-

0089), ARO DURIP (W911NF1810194) and the Arnold and Mabel Beckman foundation. J. T. Z. is supported by a National Defense Science and Engineering Graduate Fellowship. W. C. is supported by a Max Planck-Harvard Research Center for Quantum Optics fellowship. K. W. is supported by an NSF GRFP fellowship. J. M. H. is supported by the U.K. Engineering and Physical Sciences Research Council (EPSRC) Grants No. EP/N007085/1, EP/P008275/1 and EP/P01058X/1. R. G. F. acknowledges financial support of the Spanish Project FIS2017-89349-P (MINECO), and the Andalusian research group FQM-207.

* Y.Y. and K.W. contributed equally to this work.
† To whom correspondence should be addressed: ni@chemistry.harvard.edu

[1] S. S. Kondov, C.-H. Lee, K. H. Leung, C. Liedl, I. Majewska, R. Moszynski, and T. Zelevinsky, Nature Physics **15**, 1118–1122 (2019).
[2] I. Kozyryev and N. R. Hutzler, Physical Review Letters **119**, 133002 (2017), publisher: American Physical Society.
[3] V. V. Flambaum and V. A. Dzuba, Phys. Rev. A **101**, 042504 (2020).
[4] V. Andreev, D. G. Ang, D. DeMille, J. M. Doyle, G. Gabrielse, J. Haefner, N. R. Hutzler, Z. Lasner, C. Meisenhelder, B. R. O'Leary, C. D. Panda, A. D. West, E. P. West, X. Wu, and A. C. M. E. Collaboration, Nature **562**, 355 (2018).
[5] W. B. Cairncross, D. N. Gresh, M. Grau, K. C. Cossel, T. S. Roussy, Y. Ni, Y. Zhou, J. Ye, and E. A. Cornell, Phys. Rev. Lett. **119**, 153001 (2017).
[6] J. J. Hudson, D. M. Kara, I. J. Smallman, B. E. Sauer, M. R. Tarbutt, and E. A. Hinds, Nature **473**, 493 (2011).
[7] A. Micheli, G. Brennen, and P. Zoller, Nat. Phys. **2**, 341 (2006).
[8] N. Y. Yao, M. P. Zaletel, D. M. Stamper-Kurn, and A. Vishwanath, Nature Physics **14**, 405 (2018).
[9] M. L. Wall, K. R. A. Hazzard, and A. M. Rey, From atomic to mesoscale: The role of quantum coherence in systems of various complexities (World Scientific, 2015) Chap. Quantum magnetism with ultracold molecules.
[10] M. Wall, K. Maeda, and L. D. Carr, New Journal of Physics **17**, 025001 (2015).
[11] D. DeMille, Phys. Rev. Lett. **88**, 067901 (2002).
[12] K.-K. Ni, T. Rosenband, and D. D. Grimes, Chem. Sci. **9**, 6830 (2018).
[13] E. R. Hudson and W. C. Campbell, Phys. Rev. A **98**, 040302(R) (2018).
[14] Y. Lin, D. R. Leibrandt, D. Leibfried, and C.-W. Chou, Nature **581**, 273 (2020).
[15] N. Balakrishnan, J. Chem. Phys. **145**, 150901 (2016).
[16] M.-G. Hu, Y. Liu, D. D. Grimes, Y.-W. Lin, A. H. Gheorghe, R. Vexiau, N. Bouloufa-Maafa, O. Dulieu, T. Rosenband, and K.-K. Ni, Science **366**, 1111 (2019).
[17] Y. Segev, M. Pitzer, M. Karpov, N. Akerman, J. Narevicius, and E. Narevicius, Nature **572**, 189 (2019).
[18] T. de Jongh, M. Besemer, Q. Shuai, T. Karman, A. van der Avoird, G. C. Groenenboom, and S. Y. T. van de Meerakker, Science **368**, 626 (2020), https://science.sciencemag.org/content/368/6491/626.full.pdf.
[19] E. B. Norrgard, D. J. McCarron, M. H. Steinecker, M. R. Tarbutt, and D. DeMille, Phys. Rev. Lett. **116**, 063004 (2016).
[20] A. Prehn, M. Ibrügger, R. Glöckner, G. Rempe, and M. Zeppenfeld, Phys. Rev. Lett. **116**, 063005 (2016).
[21] S. Truppe, H. J. Williams, M. Hambach, L. Caldwell, N. J. Fitch, E. A. Hinds, B. E. Sauer, and M. R. Tarbutt, Nature Physics **13**, 1173 (2017).
[22] L. Anderegg, B. L. Augenbraun, Y. Bao, S. Burchesky, L. W. Cheuk, W. Ketterle, and J. M. Doyle, Nature Physics **14**, 890 (2018).
[23] S. Ding, Y. Wu, I. A. Finneran, J. J. Burau, and J. Ye, Phys. Rev. X **10**, 021049 (2020).
[24] D. Mitra, N. B. Vilas, C. Hallas, L. Anderegg, B. L. Augenbraun, L. Baum, C. Miller, S. Raval, and J. M. Doyle, Science **369**, 1366 (2020).
[25] L. De Marco, G. Valtolina, K. Matsuda, W. G. Tobias, J. P. Covey, and J. Ye, Science **363**, 853 (2019).
[26] J. T. Zhang, Y. Yu, W. B. Cairncross, K. Wang, L. R. B. Picard, J. D. Hood, Y.-W. Lin, J. M. Hutson, and K.-K. Ni, Phys. Rev. Lett. **124**, 253401 (2020).
[27] X. He, K. Wang, J. Zhuang, P. Xu, X. Gao, R. Guo, C. Sheng, M. Liu, J. Wang, J. Li, G. V. Shlyapnikov, and M. Zhan, Science **370**, 331 (2020).
[28] J. G. Danzl, E. Haller, M. Gustavsson, M. J. Mark, R. Hart, N. Bouloufa, O. Dulieu, H. Ritsch, and H.-C. Nägerl, Science **321**, 1062 (2008).
[29] K.-K. Ni, S. Ospelkaus, M. H. G. de Miranda, A. Pe'er, B. Neyenhuis, J. J. Zirbel, S. Kotochigova, P. S. Julienne, D. S. Jin, and J. Ye, Science **322**, 231 (2008).
[30] F. Lang, K. Winkler, C. Strauss, R. Grimm, and J. Hecker Denschlag, Phys. Rev. Lett. **101**, 133005 (2008).
[31] T. Takekoshi, L. Reichsöllner, A. Schindewolf, J. M. Hutson, C. R. Le Sueur, O. Dulieu, F. Ferlaino, R. Grimm, and H.-C. Nägerl, Phys. Rev. Lett. **113**, 205301 (2014).
[32] P. K. Molony, P. D. Gregory, Z. Ji, B. Lu, M. P. Köppinger, C. R. Le Sueur, C. L. Blackley, J. M. Hutson, and S. L. Cornish, Phys. Rev. Lett. **113**, 255301 (2014).
[33] J. W. Park, S. A. Will, and M. W. Zwierlein, Phys. Rev. Lett. **114**, 205302 (2015).
[34] M. Guo, B. Zhu, B. Lu, X. Ye, F. Wang, R. Vexiau, N. Bouloufa-Maafa, G. Quéméner, O. Dulieu, and D. Wang, Phys. Rev. Lett. **116**, 205303 (2016).
[35] K. K. Voges, P. Gersema, M. Meyer zum Alten Borgloh, T. A. Schulze, T. Hartmann, A. Zenesini, and S. Ospelkaus, Phys. Rev. Lett. **125**, 083401 (2020).
[36] S. Stellmer, B. Pasquiou, R. Grimm, and F. Schreck, Phys. Rev. Lett. **109**, 115302 (2012).
[37] G. Reinaudi, C. B. Osborn, M. McDonald, S. Kotochigova, and T. Zelevinsky, Phys. Rev. Lett. **109**, 115303 (2012).
[38] A. Green, H. Li, J. H. See Toh, X. Tang, K. C. McCormick, M. Li, E. Tiesinga, S. Kotochigova, and S. Gupta, Phys. Rev. X **10**, 031037 (2020).
[39] D. J. Wineland, M. Barrett, J. Britton, J. Chiaverini, B. DeMarco, W. M. Itano, B. Jelenković, C. Langer, D. Leibfried, V. Meyer, T. Rosenband, and T. Schätz, Philosophical Transactions of the Royal Society of London A: Mathematical, Physical and Engineering Sciences **361**, 1349 (2003).
[40] R. Wynar, R. S. Freeland, D. J. Han, C. Ryu, and D. J.

Heinzen, Science **287**, 1016 (2000).
[41] T. Rom, T. Best, O. Mandel, A. Widera, M. Greiner, T. W. Hänsch, and I. Bloch, Phys. Rev. Lett. **93**, 073002 (2004).
[42] M. Korek, S. Bleik, and A. R. Allouche, J. Chem. Phys. **126**, 124313 (2007).
[43] A. Grochola, P. Kowalczyk, J. Szczepkowski, W. Jastrzebski, A. Wakim, P. Zabawa, and N. P. Bigelow, Phys. Rev. A **84**, 012507 (2011).
[44] J. Zaharova, M. Tamanis, R. Ferber, A. N. Drozdova, E. A. Pazyuk, and A. V. Stolyarov, Phys. Rev. A **79**, 012508 (2009).
[45] A. Grochola, P. Kowalczyk, and W. Jastrzebski, Chemical Physics Letters **497**, 22 (2010).
[46] P. J. Zabawa, *Production of Ultracold, Absolute Vibrational Ground State NaCs Molecules*, Ph.D. thesis, University of Rochester (2012).
[47] L. R. Liu, J. T. Zhang, Y. Yu, N. R. Hutzler, Y. Liu, T. Rosenband, and K.-K. Ni, arXiv:1701.03121 (2017).
[48] F. H. Mies, E. Tiesinga, and P. S. Julienne, Phys. Rev. A **61**, 022721 (2000).
[49] J. D. Hood, Y. Yu, Y.-W. Lin, J. T. Zhang, K. Wang, L. R. Liu, B. Gao, and K.-K. Ni, Phys. Rev. Research **2**, 023108 (2020).
[50] L. R. Liu, J. D. Hood, Y. Yu, J. T. Zhang, N. R. Hutzler, T. Rosenband, and K.-K. Ni, Science **360**, 900 (2018).
[51] L. R. Liu, J. D. Hood, Y. Yu, J. T. Zhang, K. Wang, Y.-W. Lin, T. Rosenband, and K.-K. Ni, Phys. Rev. X **9**, 021039 (2019).
[52] K. Wang, X. He, R. Guo, P. Xu, C. Sheng, J. Zhuang, Z. Xiong, M. Liu, J. Wang, and M. Zhan, Phys. Rev. A **100**, 063429 (2019).
[53] This interaction shift is larger than the differential axial trapping frequency between Na and Cs atoms, which decouples the relative and center of mass motional state and improves the robustness of our preparation of the relative motional ground state.
[54] Y. Yu, *Coherent Creation of Single Molecules from Single Atoms*, Ph.D. thesis, Harvard University (2021).
[55] M. Endres, H. Bernien, A. Keesling, H. Levine, E. R. Anschuetz, A. Krajenbrink, C. Senko, V. Vuletic, M. Greiner, and M. D. Lukin, Science **354**, 1024 (2016).
[56] D. Barredo, V. Lienhard, S. de Léséleuc, T. Lahaye, and A. Browaeys, Nature **561**, 79 (2018).
[57] D. Ohl de Mello, D. Schäffner, J. Werkmann, T. Preuschoff, L. Kohfahl, M. Schlosser, and G. Birkl, Phys. Rev. Lett. **122**, 203601 (2019).